



RESEARCH

Model free adaptive control of strip temperature in continuous annealing furnace based on quantum-behaved particle swarm optimization

Hongfei Ding · Hao Shen · Ju H. Park · Qian Xie

Received: 7 May 2024 / Accepted: 26 August 2024
© The Author(s), under exclusive licence to Springer Nature B.V. 2024

Abstract This study develops a novel control scheme to address the challenge of establishing a heat transfer mechanism model for continuous annealing furnaces, which poses obstacles to the implementation of conventional model-based control strategies for regulating strip annealing temperature. The proposed approach involves integrating partial form dynamic linearization with model-free adaptive control (MFAC) using sliding time window technology to enhance adjustability and flexibility. In addition, an energy function penalty term is incorporated into the performance index function to minimize energy loss. Besides, an enhanced quantum-behaved particle swarm optimization algorithm is introduced, addressing the problems associated with parameter tuning in

the MFAC algorithm. Finally, the developed method is applied to simulate continuous annealing furnace operations in a cold rolling environment and is compared with conventional MFAC and proportional-integral-derivative control methods. The results indicate that the proposed algorithm is more efficient compared to existing algorithms, with a mean absolute error of 4.85 °C and an energy conservation rate of 4.3%.

Keywords Continuous annealing furnace · Strip temperature · Model-free adaptive control · Quantum particle swarm optimization · Partial format dynamic linearization · Energy saving control

H. Ding · H. Shen (✉)
Anhui Provincial Key Laboratory of Power Electronics and Motion Control and School of Electrical and Information Engineering, Anhui University of Technology, Ma'anshan 243032, Anhui, China
e-mail: haoshen10@gmail.com

H. Ding
School of Management Science and Technology, Anhui University of Technology, Ma'anshan 243032, Anhui, China

J. H. Park (✉)
Department of Electrical Engineering, Yeungnam University, 280 Daehak-Ro, Kyongsan 38541, Republic of Korea
e-mail: jessie@ynu.ac.kr

Q. Xie
School of Metallurgic Engineering, Anhui University of Technology, Ma'anshan 243032, Anhui, China

Q. Xie
Anhui Engineering Laboratory for Intelligent Applications and Security of Industrial Internet, Anhui University of Technology, Ma'anshan 243032, Anhui, China

1 Introduction

The continuous annealing furnace (CAF) models are a typical class of nonlinear systems, which play a crucial role in the continuous annealing treatment line for cold rolled sheet steel strips, primarily serving the purpose of strip annealing. Annealing is an essential heat treatment process in cold rolled steel strip production [1, 2], and the primary function is to reinstate the malleability of metal particles that have been previously hardened [3–6]. In CAF, the strip undergoes preheating using exhaust gas heat from both the heating furnace and soaking furnace before entering the heating section (HS) for further temperature elevation following preheating [7–9]. Each furnace area within the HS is heated by radiation tube heaters as depicted in Fig. 1 [10]. The annealing temperature of steel strip directly affects the quality of steel strip products. Therefore, accurate regulation of temperature within the HS is a critical factor in production operations [11].

The CAF exhibits intricate characteristics such as nonlinearity, substantial time delays, and robust coupling [12–14]. When there are changes in external factors or steel profiles, it is common for operation technicians to make adjustments to the furnace temperature or modify the strip speed to ensure that the strip temperature aligns with the desired heating target. However, it is noted that the furnace temperature too high can lead to several undesirable consequences that include increased fuel consumption and the strip products do not meet the required quality

standards [15]. With the progress made in modern control theory, various techniques such as PID control [16–18], fuzzy control [19, 20], adaptive control [21–23], and predictive control [24, 25] have emerged, and these techniques have been effectively applied in industrial production. For example, Agajie et al. [26] designed a novel self-tuning fuzzy PID controller for controlling frequency and power deviations in hybrid renewable energy generation systems. Elsis considered the impact of system visual uncertainty on the safety of autonomous vehicles and proposed an improved adaptive model predictive control optimization design [27]. The conventional approach used for strip temperature regulation in CAF usually employs PID controllers [28]. Despite its extensive utilization, the system fails to satisfy the performance criteria when exposed to external disturbances within the CAF, and these can result in system shocks or longer adjustment times, ultimately affecting the quality of the steel strip. To address these issues, Wu et al. introduced a nonlinear model predictive control (MPC) method to enhance the accuracy of adjusting strip temperature in CAF [29]. Niederer et al. [30] proposed a nonlinear model predictive controller to regulate strip temperature in CAF with mixed combustion combinations. However, the availability of accurate model information becomes crucial when employing MPC. Nevertheless, the absence of on-site measurement sensors introduces numerous unknown parameters into the CAF posing challenges in accurately predicting outcomes through mathematical models. Consequently, to efficiently regulate a

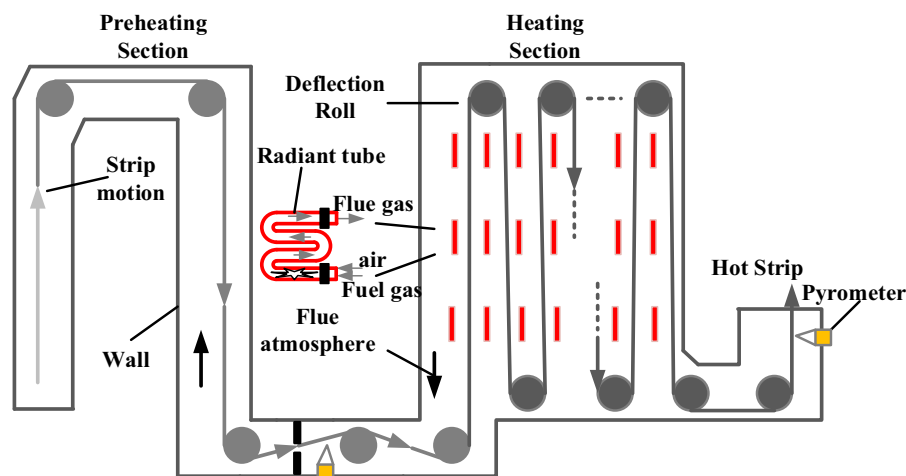


Fig. 1 Process diagram of heating section of continuous annealing furnace

complex system such as a CAF, it is essential to modify the model and decrease the level of control complexity. In this study, a novel partial form dynamic linearization data model based MFAC (PFDL-MFAC) scheme is proposed as an effective method to deal with the above problems.

MFAC is a well-known control approach that relies on data-driven techniques and does not require detailed knowledge of the controlled system [31]. On the contrary, the design and implementation of this method completely depend on real-time input and output (I/O) data, and effectively solving the parameter tuning problem of PID control when dealing with complex systems. Additionally, this study considers the energy loss index of CAFs to mitigate energy wastage. However, the majority of current PFDL-MFAC schemes commonly employ fixed controller parameters, which offer operational simplicity but lack adaptability to the dynamic changes of the system [32]. Metaheuristic algorithms, including genetic algorithms, particle swarm optimization (PSO), and others, belong to a category of algorithms that draw inspiration from natural phenomena or biological behaviors. They are employed to address optimization problems and find applications in industrial production. For instance, in [33], a novel cooperative optimization algorithm is employed to improve the trajectory tracking of robotic arms. In [34], a combination of fuzzy logic and Harris Hawks optimization algorithm is utilized to achieve the optimal energy management strategy for a seawater desalination plant. Metaheuristic algorithms are also commonly used to optimize the parameters of controllers. Essa et al. [35] proposed an intelligent tuning method for MPC based on the Bat algorithm to enhance the control accuracy for aircraft flight control problems. Bergies et al. [36] addressed the issue of uncertainties in autonomous vehicle steering angle adjustments caused by road undulations and visual system dynamics, employing a dandelion optimization strategy to obtain the optimal parameters for MPC. To address the parameters tuning issue of model-free adaptive controllers, an enhanced QPSO (EQPSO) algorithm, which dynamically adjusts controller parameters using real-time I/O information is utilized in this study [37]. The QPSO algorithm, which incorporates principles derived from quantum theory, is an advanced iteration of the particle swarm optimization algorithm. When compared with other intelligent algorithms, this algorithm does not require the calculation of particle velocity, has fewer

control parameters, and offers faster convergence speed [38, 39]. Hence, this study introduces an enhanced QPSO algorithm that integrates the differential evolution algorithm (DE) and generalized opposition-based learning (GOBL) to dynamically optimize the parameters of the model-free adaptive controller [40, 41]. By integrating the parameters of PFDL-MFAC as variables for optimization within the EQPSO algorithm and utilizing a newly proposed fitness function, optimal values are chosen to attain enhanced performance in accordance with the current system conditions.

Based on the aforementioned analysis, this study presents an improved PFDL-MFAC approach for the regulation of strip temperature in CAF. In contrast to currently available technologies, this study presents several distinct advantages as follows.

1. A novel methodology has been devised to optimize the parameters of a model-free adaptive controller. This methodology enhances the quantum particle swarm algorithm to address its limitations, such as slow convergence and a tendency to produce local optima. The refined algorithm is then used to dynamically adjust the parameters of the PFDL-MFAC controller based on changes in steel strip specifications, effectively solving the parameter calibration challenge.
2. Compared to the findings in reference [29], this study posits that the continuous annealing furnace functions as a high-energy-consuming apparatus. To address this, an energy penalty term has been integrated into the performance index function of the controller within the framework of the steel strip annealing temperature control scheme. The primary objective of this integration is to promote energy conservation and emission reduction. Notably, this aspect is rarely considered in other control strategy studies.
3. In contrast to the research conducted in reference [30], a model-free adaptive control approach utilizing data-driven technology is introduced to tackle the challenge of strip temperature regulation in continuous annealing furnaces. This method aims to overcome the limitations of conventional controllers that heavily depend on mathematical models.

Notation In this study, all the real numbers and positive integers are represented by \mathbb{R} and \mathbb{Z}^+ ; $\| \cdot \|$ denotes Euclidean norm of vectors or matrices; *sign*

indicates symbolic function; $rand(r_1, r_2)$ denotes the random number uniformly distributed in the interval (r_1, r_2) ; and \parallel represent the ‘AND’ and ‘OR’ relationships of an equation, respectively.

2 Prediction model for the strip temperature of CAF

The derivation of a mathematical model for CAFs is challenging due to their complex and nonlinear relationships, which makes mechanism modeling difficult. The analysis of the process principle of a CAF shows that the strip temperature is influenced by various significant factors, including strip width, strip thickness, production speed, furnace temperature, and air–fuel ratio. This study utilizes autoregressive moving average (ARMA) modeling theory and considers temporal characteristics, to forecast the dynamic model of strip temperature.

Remark 1 The control scheme implemented in this study does not incorporate any information from the established model, which solely depends on the predicted model to generate the required output data for controller design, without actively engaging in the controller design process.

The modeling data utilized in this study were obtained from real-time CAF data collected at the production site. The ARMA model of CAF is simplified as

$$\Upsilon^a(z^{-1})T(k) = \Upsilon^b(z^{-1})u(k) \tag{1}$$

where $u(k)$ and $T(k)$ are the input and output variables, respectively; k denotes the sampling time; $\Upsilon^a(z^{-1}), \Upsilon^b(z^{-1})$ are shown in (2).

$$\begin{cases} \Upsilon^a(z^{-1}) = I + \Upsilon_1^a z^{-1} + \Upsilon_2^a z^{-2} + \dots + \Upsilon_{n_a}^a z^{-n_a} \\ \Upsilon^b(z^{-1}) = \Upsilon_1^b z^{-1} + \Upsilon_2^b z^{-2} + \dots + \Upsilon_{n_b}^b z^{-n_b} \end{cases} \tag{2}$$

where I is the identity matrix; n_a and n_b represent the dimensions of the matrices Υ^a and Υ^b , respectively.

In this study, an experiment was conducted to collect production data from the CAF within a specified period on the continuous annealing line. The sampling time interval was configured to one minute, and a total of 4800 consecutive data sets were

chosen. The initial 2400 data sets were selected for training, while the remaining data sets were reserved for testing. By conducting experiments, the values of $\Upsilon^a(z), \Upsilon^b(z)$ are obtained as

$$\begin{aligned} \Upsilon^a(z) &= 1 - 0.902z^{-1}, \Upsilon^b(z) \\ &= \begin{bmatrix} -0.06116z^{-1} + 0.05815z^{-2}, 0.03834z^{-1} - 0.03201z^{-2}, \\ 0.05552z^{-1} + 0.02338z^{-2}, 0.008416z^{-1} - 0.002905z^{-2} \end{bmatrix}. \end{aligned}$$

3 A design of partial form dynamic linearization-improved model-free adaptive control (PFDL-IMFAC)

The PFDL-IMFAC control scheme is a proposed energy-saving solution for CAF. It is developed by integrating the MFAC and PFDL data models, as well as incorporating constraints on energy consumption. This algorithm takes into account not only the tracking error of strip temperature but also addresses the issue of energy loss that occurs during continuous annealing. Meanwhile, the EQPSO optimization algorithm is employed to optimize the parameters of the PFDL-IMFAC method.

3.1 Dynamic linearization

The strip temperature in the CAF is not solely determined by a single control input at any given moment. By linearizing, it becomes possible to analyze the effects of various input changes within a predetermined time frame on subsequent output changes. The aforementioned methodology is referred to as the PFDL data processing method, which is capable of capturing intricate dynamics in the original system, while simultaneously mitigating system complexity through dynamic linearization.

For the nonlinear system of CAF, the dynamic equation can be established as follows

$$T(k + 1) = f(T(k), \dots, T(k - n_T), u(k), \dots, u(k - n_u)) \tag{3}$$

where $u(k) \in \mathbb{R}^m$ and $T(k) \in \mathbb{R}^n$, respectively; n_u and n_T denote the orders of the input and output, respectively; $f(\cdot)$ represents the nonlinear time-varying function. $\bar{U}_q(k) \in \mathbb{R}^{m_q}$ is defined as

$$\bar{U}_q(k) = [u^T(k), \dots, u^T(k - q + 1)]^T \tag{4}$$

which satisfies $\bar{U}_q(k) = 0_q$, when $k \leq 0$, where $q \in \mathbb{Z}^+$ represents the integer length of the linearized control input. For system (3), two assumptions can be established as follows:

Assumption 1 The nonlinear time-varying function $f(\cdot)$ possesses continuous partial derivatives with respect to input $u(k), u(k - 1), \dots, u(k - q + 1)$, respectively.

Assumption 2 The system (3) satisfies the generalized Lipschitz condition, which guarantees that for any given time interval $k_1 \neq k_2 \geq 0$ and $\bar{U}_q(k_1) \neq \bar{U}_q(k_2)$, there exists a positive constant b meets $\|T(k_1 + 1) - T(k_2 + 1)\| \leq b\|\bar{U}_q(k_1) - \bar{U}_q(k_2)\|$, and $\Delta\bar{U}_q(k) = \bar{U}_q(k) - \bar{U}_q(k - 1)$ is precisely defined.

Remark 2 Assumption 1 is a common constraint in CAF controller design, while Assumption 2 sets a limit on the maximum rate of output change of the CAF. Theorem 1 can be derived from Assumptions 1 and 2.

Theorem 1 The nonlinear time-varying system (3) which satisfying Assumptions 1 and 2 can be transformed into a PFDL model as shown in (5) by introducing a time-varying pseudo-Jacobian block matrix (PJM) $\Xi_{pq}(k)$ when $\|\Delta\bar{U}_q(k)\| \neq 0$ is given for a positive integer q .

$$T(k + 1) = T(k) + \Xi_{pq}(k)\Delta\bar{U}_q(k) \tag{5}$$

For any given time, $\Xi_{pq}(k) = [\Xi_1(k), \dots, \Xi_q(k)]$ varies within a bounded range, and its corresponding sub-square matrix can be expressed as

$$\Xi_i(k) = \begin{bmatrix} \Xi_{11i}(k) & \Xi_{12i}(k) & \cdots & \Xi_{1n_i}(k) \\ \Xi_{21i}(k) & \Xi_{22i}(k) & \cdots & \Xi_{2n_i}(k) \\ \vdots & \vdots & \ddots & \vdots \\ \Xi_{n_i1i}(k) & \Xi_{n_i2i}(k) & \cdots & \Xi_{n_in_i}(k) \end{bmatrix}, \tag{6}$$

$i = 1, \dots, q.$

Proof Theorem 1 has been rigorously proven in [31], demonstrating that different PFDL data models can be obtained by selecting various values of q .

3.2 Control design

The inclusion of the penalty term in the energy function is a key aspect addressed in this study, therefore, the new performance index function is selected by PFDL-IMFAC as follows

$$J(u(k)) = \|T_m(k + 1) - T(k + 1)\|^2 + \xi\|u(k) - u(k - 1)\|^2 + \zeta\|u(k)\|^2. \tag{7}$$

The output $T_m(k + 1)$ serves as the reference of strip temperature, and $\xi > 0$ acts as the weight factor to restrict changes in control input. The role of $\zeta\|u(k)\|^2$ is to minimize energy loss in CAF.

Remark 3 The index function in (7) evaluates the control performance, stability, and fuel consumption management capability of the strip temperature control system.

Substituting (5) into (7) obtains

$$J(u(k)) = \|T_m(k + 1) - T(k + 1) - \Xi_{pq}(k)\Delta\bar{U}_q(k)\|^2 + \xi\|u(k) - u(k - 1)\|^2 + \zeta\|u(k)\|^2. \tag{8}$$

Taking the first-order partial derivative of (8) with respect to $u(k)$ is

$$\left(\xi I + \Xi_1^T(t)\Xi_1(t) \right) \Delta u(k) + \zeta u(k) - \Xi_1^T(t) \left(T_m(k + 1) - T(k) - \sum_{i=2}^q \Xi_i(t)\Delta u(k - i + 1) \right) = 0. \tag{9}$$

Due to the matrix inversion involved in (9), it is challenging to compute for high-dimensional systems. To address this issue, a simplified algorithm is proposed by referring to the control algorithm for a single output, $u(k)$ is proposed as

$$u(k) = \frac{\left(\xi + \|\Xi_1(k)\|^2 \right) u(k - 1) + \Xi_1^T(k)\rho_1(T_m(k + 1) - T(k))}{\xi + \|\Xi_1(k)\|^2 + \zeta} - \frac{\Xi_1^T(k) \sum_{i=2}^q \rho_i \Xi_i(k)\Delta u(k - i + 1)}{\xi + \|\Xi_1(k)\|^2 + \zeta} \tag{10}$$

where $\rho_i \in (0, 1]$ is used to enhance the generality of the PFDL-IMFAC algorithm.

The real-time estimation of $\Xi_{pq}(k)$ is achieved by introducing the parameter estimation criterion function as follows

$$J(\Xi_{pq}(k)) = \|\Delta T(k) - \Xi_{pq}(k)\Delta\bar{U}_q(k-1)\|^2 + \mu \|\Xi_{pq}(k) - \hat{\Xi}_{pq}(k)\|^2 \tag{11}$$

where $\mu > 0$ is used to constrain the rate of variation among adjacent parameters.

The estimation algorithm of $\Xi_{pq}(k)$ can be derived as

$$\hat{\Xi}_{pq}(k) = \hat{\Xi}_{pq}(k-1) + \eta(\Delta T(k) - \hat{\Xi}_{pq}(k-1)\Delta\bar{U}_q(k-1)) \frac{\Delta\bar{U}_q^T(k-1)}{\mu + \|\Delta\bar{U}_q(k-1)\|^2} \tag{12}$$

where $\hat{\Xi}_{pq}(k) = [\hat{\Xi}_1(k), \dots, \hat{\Xi}_q(k)]^T$ is the estimated value of $\Xi_{pq}(k)$; $\eta \in (0, 2]$ is the step factor.

To enhance the robustness of the PJM parameter estimation algorithm, a parameter reset algorithm (13) is introduced.

$$\begin{cases} \hat{\Xi}_{ii1}(k) = \hat{\Xi}_{ii1}(1), |\hat{\Xi}_{ii1}(1)| < b_2 \|\hat{\Xi}_{ii1}(1)\| \\ \quad > ab_2 \|\text{sign}(\hat{\Xi}_{ii1}(k)) \neq \text{sign}(\hat{\Xi}_{ii1}(1))\| \\ \hat{\Xi}_{ij1}(k) = \hat{\Xi}_{ij1}(1), |\hat{\Xi}_{ij1}(1)| > b_1 \|\text{sign}(\hat{\Xi}_{ij1}(k)) \neq \text{sign}(\hat{\Xi}_{ij1}(1))\| \end{cases} \tag{13}$$

where b_1 and b_2 represent small positive numbers that satisfy the condition $|\Xi_{ij1}(t)| \leq b_1, b_2 \leq |\Xi_{ii1}(t)| \leq ab_2, 1 \leq a$; $\hat{\Xi}_{ii1}(1)$ and $\hat{\Xi}_{ij1}(1)$ are the initial values of $\hat{\Xi}_{ii1}(k)$ and $\hat{\Xi}_{ij1}(k)$, respectively.

According to (3) and (10), it is possible to calculate the strip temperature. Meanwhile, it has been demonstrated by (10) that the energy-saving control algorithm of the CAF is dependent solely on the furnace temperature.

Remark 4 The selection of different control inputs for linearizing the length of the constant q results in distinct PFDL data models. By judiciously choosing q and $\Xi_{pq}(k)$, the flexibility of the dynamic linearized data model can be enhanced to accurately represent the original nonlinear system.

3.3 Stability analysis of PFDL-IMFAC

The boundedness of $\Xi_{pq}(k)$ has been established, and the convergence of the system output error is subsequently proven. For ease of explanation, the stability analysis for the case $n_u = 1, n_T = 1, q = 1$ is provided below, with a similar proof procedure applicable to other cases [42].

According to (10), the control law at $n_u = 1, n_T = 1, q = 1$ is expressed as

$$u(k) = \frac{\xi + \hat{\Xi}^2(k)}{\xi + \hat{\Xi}^2(k) + \zeta} u(k-1) + \frac{\rho \hat{\Xi}(k)}{\xi + \hat{\Xi}^2(k) + \zeta} e(k) \tag{14}$$

where $\hat{\Xi}(k)$ is the estimated value of the time-varying parameter $\Xi(k)$.

Assumption 3 The partial derivative of the nonlinear time-varying function $f(\cdot)$ with respect to the system input $u(k)$ remains continuous for a single-input single-output system in the form (3).

Assumption 4 The system satisfies the generalized Lipschitz condition for any time $0 \leq k_1 \neq k_2$, and supposes that $u(k_1) \neq u(k_2)$, where $|T(k_1 + 1) - T(k_2 + 1)| \leq b|u(k_1) - u(k_2)|$ exists. Here, b represents a positive constant.

Lemma 1 The output error will converge to a constant ψ , i.e. $\lim_{k \rightarrow \infty} |e(k)| \leq \psi$, which is related to ζ , if the nonlinear time-varying system satisfies Assumptions 3 and 4, and the control method is employed as in (10).

Proof Define the output error as

$$e(k) = T_m(k) - T(k). \tag{15}$$

From (15) and $\Delta T(k+1) = \Xi(k)\Delta u(k)$, we get

$$e(k+1) = T_m(k) - T(k) - \Xi(k)\Delta u(k) = e(k) - \Xi(k)\Delta u(k). \tag{16}$$

Then, (14) can be rewritten as

$$\Delta u(k) = -\frac{\zeta}{\xi + \hat{\Xi}^2(k) + \zeta} u(k-1) + \frac{\rho \hat{\Xi}(k)}{\xi + \hat{\Xi}^2(k) + \zeta} e(k). \tag{17}$$

Substituting (17) into (16) obtains

$$\begin{aligned}
 e(k+1) &= e(k) - \Xi(k)\Delta u(k) \\
 &= \left(1 - \frac{\rho\hat{\Xi}(k)\Xi(k)}{\xi + \hat{\Xi}^2(k) + \zeta}\right)e(k) \\
 &\quad + \frac{\zeta\Xi(k)}{\xi + \hat{\Xi}^2(k) + \zeta}u(k-1).
 \end{aligned}
 \tag{18}$$

According to (14), the $u(k-1)$ is defined as

$$\begin{aligned}
 u(k-1) &= \frac{\xi + \hat{\Xi}^2(k-1)}{\xi + \hat{\Xi}^2(k-1) + \zeta}u(k-2) \\
 &\quad + \frac{\rho\hat{\Xi}(k-1)}{\xi + \hat{\Xi}^2(k-1) + \zeta}e(k-1).
 \end{aligned}
 \tag{19}$$

Substituting (19) into (18) gives

$$\begin{aligned}
 e(k+1) &= \left(1 - \frac{\rho\hat{\Xi}(k)\Xi(k)}{\xi + \hat{\Xi}^2(k) + \zeta}\right)e(k) + \frac{\zeta\Xi(k)}{\xi + \hat{\Xi}^2(k) + \zeta} \\
 &\quad \left(\frac{\xi + \hat{\Xi}^2(k-1)}{\xi + \hat{\Xi}^2(k-1) + \zeta}u(k-2) + \frac{\rho\hat{\Xi}(k-1)}{\xi + \hat{\Xi}^2(k-1) + \zeta}e(k-1)\right) \\
 &\leq \tau_1 e(k) + \tau_2 \tau_4 \sum_{j=1}^{k-1} \tau_3^{k-1-j} e(j) + \tau_2 \tau_3^{k-1} u(0)
 \end{aligned}
 \tag{20}$$

where

$$\begin{cases}
 \tau_1 = \max\left(\left|1 - \frac{\rho\hat{\Xi}(k)\Xi(k)}{\xi + \hat{\Xi}^2(k) + \zeta}\right|, \dots, \left|1 - \frac{\rho\hat{\Xi}(1)\Xi(1)}{\xi + \hat{\Xi}^2(1) + \zeta}\right|\right), \\
 \tau_2 = \max\left(\left|\frac{\zeta\Xi(k)}{\xi + \hat{\Xi}^2(k) + \zeta}\right|, \dots, \left|\frac{\zeta\Xi(1)}{\xi + \hat{\Xi}^2(1) + \zeta}\right|\right), \\
 \tau_3 = \max\left(\left|\frac{\xi + \hat{\Xi}^2(k-1)}{\xi + \hat{\Xi}^2(k-1) + \zeta}\right|, \dots, \left|\frac{\xi + \hat{\Xi}^2(1)}{\xi + \hat{\Xi}^2(1) + \zeta}\right|\right), \\
 \tau_4 = \max\left(\left|\frac{\rho\hat{\Xi}(k-1)}{\xi + \hat{\Xi}^2(k-1) + \zeta}\right|, \dots, \left|\frac{\rho\hat{\Xi}(1)}{\xi + \hat{\Xi}^2(1) + \zeta}\right|\right)
 \end{cases}$$

Taking the absolute value on both sides of (20) as

$$\begin{aligned}
 |e(k+1)| &\leq \tau_1 |e(k)| + \tau_2 \tau_4 \sum_{j=1}^{k-1} \tau_3^{k-1-j} |e(j)| \\
 &\quad + \tau_2 \tau_3^{k-1} |u(0)|.
 \end{aligned}
 \tag{21}$$

It can be deduced that

$$\begin{aligned}
 |e(k)| &\leq \tau_1 |e(k-1)| + \tau_2 \tau_4 \sum_{j=1}^{k-2} \tau_3^{k-2-j} |e(j)| \\
 &\quad + \tau_2 \tau_3^{k-2} |u(0)|.
 \end{aligned}
 \tag{22}$$

Substituting (22) into (21) yields

$$\begin{aligned}
 |e(k+1)| &\leq \tau_1^2 |e(k-1)| + \tau_1 \tau_2 \tau_4 \sum_{j=1}^{k-2} \tau_3^{k-2-j} |e(j)| \\
 &\quad + \tau_2 \tau_4 \sum_{j=1}^{k-1} \tau_3^{k-1-j} |e(j)| + \tau_1 \tau_2 \tau_3^{k-2} |u(0)| \\
 &\quad + \tau_2 \tau_3^{k-1} |u(0)|.
 \end{aligned}
 \tag{23}$$

In the same way, the output error inequality of other processes gives

$$\begin{cases}
 |e(k-1)| \leq \tau_1 |e(k-2)| + \tau_2 \tau_4 \sum_{j=1}^{k-3} \tau_3^{k-3-j} |e(j)| \\
 \quad + \tau_2 \tau_3^{k-3} |u(0)| \\
 |e(k-2)| \leq \tau_1 |e(k-3)| + \tau_2 \tau_4 \sum_{j=1}^{k-4} \tau_3^{k-4-j} |e(j)| \\
 \quad + \tau_2 \tau_3^{k-4} |u(0)| \\
 \vdots \\
 |e(2)| \leq \tau_1 |e(1)| + \tau_2 \tau_4 |e(0)| + \tau_2 \tau_3 |u(0)|.
 \end{cases}
 \tag{24}$$

Substituting (24) into (23) yields

$$\begin{aligned}
 |e(k+1)| &\leq \tau_1^2 |e(k-1)| \\
 &\quad + \tau_1 \tau_2 \tau_4 \sum_{j=1}^{k-2} \tau_3^{k-2-j} |e(j)| \\
 &\quad + \tau_2 \tau_4 \sum_{j=1}^{k-1} \tau_3^{k-1-j} |e(j)| + \tau_1 \tau_2 \tau_3^{k-2} |u(0)| \\
 &\quad + \tau_2 \tau_3^{k-1} |u(0)|, \dots, \leq \tau_1^k |e(1)| \\
 &\quad + \tau_2 \tau_4 \sum_{m=1}^{k-1} \tau_1^m \sum_{j=1}^{k-m-1} \tau_3^{k-m-1-j} |e(j)| \\
 &\quad + \tau_2 |u(0)| \sum_{m=1}^{k-1} \tau_1^m \tau_3^{k-m-1}.
 \end{aligned}
 \tag{25}$$

Define

$$\begin{aligned}
 h(k+1) &= \tau_1^k |e(1)| + \tau_2 \tau_4 \sum_{m=1}^{k-1} \tau_1^m \\
 &\quad \sum_{j=1}^{k-m-1} \tau_3^{k-m-1-j} |e(j)| \\
 &\quad + \tau_2 |u(0)| \sum_{m=1}^{k-1} \tau_1^m \tau_3^{k-m-1}.
 \end{aligned}
 \tag{26}$$

For $h(k + 1)$, the (27) holds

$$\begin{aligned}
 h(k + 2) &= \tau_1^{k+1}|e(1)| + \tau_2\tau_4 \sum_{m=1}^k \tau_1^m \sum_{j=1}^{k-m} \tau_3^{k-m-j}|e(j)| \\
 &\quad + \tau_2|u(0)| \sum_{m=1}^k \tau_1^m \tau_3^{k-m} \\
 &\leq \tau_1^{k+1}|e(1)| + \tau_2\tau_4 \sum_{m=1}^{k-1} \tau_1^m \sum_{j=1}^{k-m-1} \tau_3^{k-m-j-1}|e(j)| \\
 &\quad + \tau_2|u(0)| \sum_{m=1}^{k-1} \tau_1^m \tau_3^{k-m-1} + \tau_2|u(0)|\tau_1^k.
 \end{aligned} \tag{27}$$

The boundedness of pseudo-partial derivatives (PPD) is introduced, and demonstrating that for any time k , $\Xi(k)$ is always less than the constant \bar{b}_2 . The proof of this boundedness has been established in [34].

Define $\zeta_{\min} + \zeta_{\min} = 0.25\bar{b}_2$ and then select $\zeta_{\min} + \zeta_{\min} < \zeta + \zeta$. The existence of a constant M_1 is necessary for the validity of the following inequality

$$\begin{aligned}
 0 < M_1 &\leq \frac{\hat{\Xi}(k)\Xi(k)}{\zeta + \hat{\Xi}^2(k) + \zeta} \leq \frac{\bar{b}_2\hat{\Xi}(k)}{\zeta + \hat{\Xi}^2(k) + \zeta} \\
 &\leq \frac{\bar{b}_2\hat{\Xi}(k)}{2\sqrt{\zeta} + \zeta\hat{\Xi}(k)} < \frac{\bar{b}_2}{2\sqrt{\zeta_{\min}} + \zeta_{\min}} = 1.
 \end{aligned} \tag{28}$$

According to (28) and $\rho \in (0, 1]$, (29) holds

$$\tau_1 = \max \left(\left| 1 - \frac{\rho\hat{\Xi}(k)\Xi(k)}{\zeta + \hat{\Xi}^2(k) + \zeta} \right|, \dots, \left| 1 - \frac{\rho\hat{\Xi}(1)\Xi(1)}{\zeta + \hat{\Xi}^2(1) + \zeta} \right| \right) \leq |1 - \rho M_1| < 1. \tag{29}$$

Because of $0 < \tau_1 < 1$, (27) can be further simplified as

$$\begin{aligned}
 h(k + 2) &\leq \tau_1\tau_1^k|e(1)| + \tau_2\tau_4 \sum_{m=1}^{k-1} \tau_1^m \\
 &\quad \sum_{j=1}^{k-m-1} \tau_3^{k-m-j-1}|e(j)| + \tau_2|u(0)| \sum_{m=1}^{k-1} \tau_1^m \tau_3^{k-m-1} \\
 &\quad + \tau_2|u(0)|\tau_1^k \\
 &\leq \tau_1^k|e(1)| + \tau_2\tau_4 \sum_{m=1}^{k-1} \tau_1^m \sum_{j=1}^{k-m-1} \tau_3^{k-m-j-1}|e(j)| \\
 &\quad + \tau_2|u(0)| \sum_{m=1}^{k-1} \tau_1^m \tau_3^{k-m-1} + \tau_2|u(0)|\tau_1^k < h(k + 1) \\
 &\quad + \tau_2|u(0)|\tau_1^k.
 \end{aligned} \tag{30}$$

The existence of $0 < M_2 < 1$ is necessary for (31) to hold as stated

$$h(k + 2) < M_2h(k + 1) + \tau_2|u(0)|\tau_1^k. \tag{31}$$

The following relation can thus be deduced

$$h(k + 1) < M_2h(k) + \tau_2|u(0)|\tau_1^{k-1}. \tag{32}$$

Combining (31) and (32) obtains

$$\begin{aligned}
 h(k + 2) &< M_2h(k + 1) + u(0)\tau_2\tau_1^k < M_2^2h(k) \\
 &\quad + u(0)\tau_2\tau_1^k + M_2u(0)\tau_2\tau_1^{k-1} < \dots < M_2^{k+1}h(1) \\
 &\quad + u(0)\tau_2\tau_1 + \dots + u(0)\tau_2\tau_1^k < M_2^{k+1}h(1) \\
 &\quad + u(0)\tau_2 \frac{\tau_1(1 - \tau_1^k)}{1 - \tau_1}.
 \end{aligned} \tag{33}$$

Because $0 < M_2 < 1$, the result is

$$\lim_{k \rightarrow \infty} h(k + 2) = \lim_{k \rightarrow \infty} |e(k + 2)| \leq \frac{u(0)\tau_2\tau_1}{1 - \tau_1}. \tag{34}$$

Thus, let $\psi = \frac{u(0)\tau_2\tau_1}{1 - \tau_1}$, Theorem 1 be proved to hold, i.e. $\lim_{k \rightarrow \infty} |e(k)| \leq \psi$.

3.4 EQPSO algorithm design

The PFDL-IMFAC algorithm proposed in this study encompasses a substantial number of parameters. However, the conventional method of manually adjusting these parameters not only incurs a significant time cost but also fails to attain optimal control performance. Therefore, this study utilizes the benefits of EQPSO to optimize the control parameters of PFDL-IMFAC.

The initial position of particles randomly generated within the search range is shown in (35). The position of i th particle and the dimension of the particle are defined as $X_i = (x_{i1}, x_{i2}, \dots, x_{iD})$ and D , respectively. According to the upper and lower bound constraints, the particle position is limited within the specified search range.

$$\begin{aligned}
 x_{ij}(0) &= x_{ij}^{low} + rand \left(x_{ij}^{up} - x_{ij}^{low} \right), \\
 \left\{ x_{ij}(0) | x_{ij}^{low} \leq x_{ij}(0) \leq x_{ij}^{up} \right\}, \\
 (i &= 1, 2, \dots, M; j = 1, 2, \dots, D)
 \end{aligned} \tag{35}$$

where $x_{ij}(0)$ is the j th component of the i th individual in the initial population; M denotes the population

size; x_{ij}^{low} and x_{ij}^{up} represent the upper and lower limits of the population position, respectively.

The average optimal position of the particle swarm Z_{mbst}^t is calculated by

$$Z_{mbst}^t = \frac{\sum_{i=1}^M \frac{Z_i(t)}{f_{bst}^i}}{\sum_{i=1}^M \frac{1}{f_{bst}^i}} \tag{36}$$

where $Z_i(t)$ denotes the historical optimal position of an individual particle; f_{bst}^i represents the fitness value corresponding to the historical best position of the i th particle at the t th iteration, and the fitness calculation formula is

$$f(X_i(t)) = \sqrt{\frac{1}{M} \sum_{i=1}^M (Y_i(X_i(t)) - T_{ms})^2} \tag{37}$$

where $X_i(t)$ denotes the position of the particle; $Y_i(X_i^t)$ and T_{ms} are the actual values and target values obtained after parameter optimization, respectively.

The attractor $z_i(t)$ of the particle is

$$z_i(t) = t_i^t \times Z_i(t) + (1 - t_i^t) \times Z_g(t), t_i^t \in rand(0, 1) \tag{38}$$

where $Z_g(t)$ represents the global historical optimal position of the particle swarm.

The particle position is updated by

$$X_i(t) = \begin{cases} z_i(t) - \gamma |Z_{mbst}^t - X_i(t)| \ln \left| \frac{1}{\chi_i(t)} \right|, & 0 < \chi_i(t) \leq 0.5 \\ z_i(t) + \gamma |Z_{mbst}^t - X_i(t)| \ln \left| \frac{1}{\chi_i(t)} \right|, & 0.5 < \chi_i(t) \leq 1 \end{cases} \tag{39}$$

where γ is used to regulate the convergence speed of the particles, and defined as

$$\gamma = (\gamma_a - \gamma_b) \cdot \frac{I_{max} - t}{I_{max}} + \gamma_b \tag{40}$$

where I_{max} is the maximum number of iterations; $\gamma \in [\gamma_a, \gamma_b]$ and $\{\gamma_a, \gamma_b \in \mathbb{Z}^+ | \gamma_b > \gamma_a\}$.

Remark 5 Although the QPSO algorithm enhances the global optimization capability of particles to some extent, it tends to generate local optimal solutions due to its inherent characteristics. To enhance the global search capability of particles in the QPSO algorithm, this study proposes an improved search strategy.

The search strategy of the QPSO algorithm is initially proposed by incorporating DE, which employs the mechanisms of crossover, mutation, and selection mechanisms to update the population, thereby facilitating algorithm optimization through iterative population evolution.

The DE algorithm randomly selects two distinct individuals from the current population, and generates the mutation operator using the difference method as follows

$$v_{ij}(t) = x_{r_1,j}(t) + \varpi_z (x_{r_2,j}(t) - x_{r_1,j}(t)) \tag{41}$$

where $r_1 \neq r_2$, and $r_1, r_2 \in [1, M]$ are all random integers; ϖ_z represents the scaling factor.

To ensure that ϖ_z becomes a non-repeated pseudo-random number within the interval $[0, 1]$, the sinusoidal chaotic random sequence is utilized by

$$\varpi_z(I_{ev}) = \sin^2 \left(h_v \arcsin \sqrt{\varpi_z(I_{ev} - 1)} \right), \varpi_z(0) \in rand(0, 1) \tag{42}$$

where I_{ev} denotes the evolutionary algebra; $h_v > 1$ is a constant.

The individuals $x_j(t)$ and $v_i(t)$ were subjected to a cross, resulting in the acquisition of the experimental individual $w_{ij}(t)$ as follows

$$w_{ij}(t) = \begin{cases} v_{ij}(t), & \text{while } : rand(0, 1) \leq P_{ev} \ \& \ j = j_d \\ x_{ij}(t), & \text{other} \end{cases} \tag{43}$$

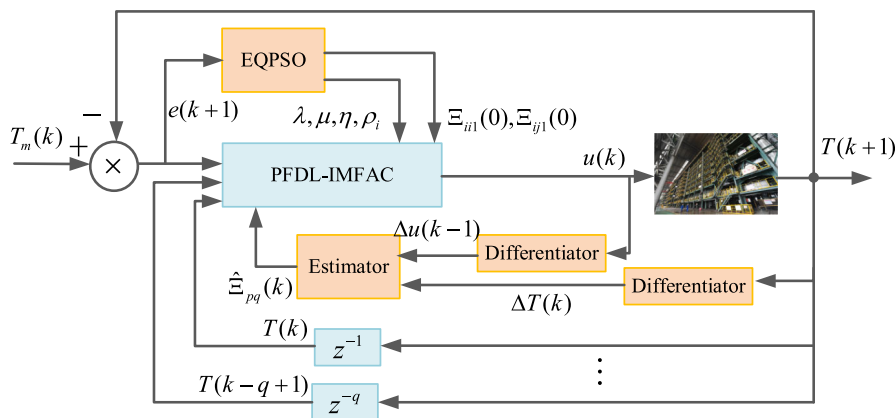
where P_{ev} is the crossover probability, and $P_{ev} \in [0.8, 1]$; $j_d \in \{1, 2, \dots, D\}$ is a random integer.

The greedy strategy is used to choose the one with lower fitness as the next generation by (44).

$$x_{ij}(t+1) = \begin{cases} w_{ij}(t), & \text{while } f(w_{ij}(t)) \leq f(x_{ij}(t)) \\ x_{ij}(t), & \text{other} \end{cases} \tag{44}$$

The use of the difference operator in the DE algorithm effectively maintains population diversity, thus enhancing its overall performance. Additionally, the incorporation of crossover and selection operators further enhances the ability of the local search. However, the efficiency of the DE algorithm gradually decreases during its operation. To solve this problem, the GOBL algorithm is integrated into QPSO, along with a dynamically updated search boundary, to

Fig. 2 The strip temperature control scheme based on EQPSO for PFDL-IMFAC



enhance the likelihood of discovering the global optimal solution.

The reverse solution X_i^{op} of X_i can be obtained by

$$\begin{cases} X_i^{op} = k_{op}(\Psi_{up}^t + \Psi_{low}^t) - X_i^t, & k_{op} = rand(0, 1) \\ X_i^{op} = rand[\Psi_{low}^t, \Psi_{up}^t], & \text{if } X_i^{op} < \Psi_{low}^t \parallel X_i^{op} > \Psi_{up}^t \\ X_i^{op} = rand[\Psi_{low}^t, \Psi_{up}^t], & \text{if } X_i^{op} < X_{min} \parallel X_i^{op} > X_{max} \end{cases} \quad (45)$$

where Ψ_{up}^t and Ψ_{low}^t represent the upper and lower bounds of the generalized inverse solution produced, respectively; $[X_{min}, X_{max}]$ is the upper and lower bounds on the search space.

By incorporating the concepts of DE and GOBL, the global search capability of QPSO is significantly reinforced. The pseudo-code algorithm procedure of the EQPSO is revealed in Algorithm 1.

The main steps of the EQPSO algorithm pseudo code

Algorithm 1 The main steps of the EQPSO algorithm pseudo code

1. The initialization process involves randomly generating the initial positions of a set of particles and the number of EQPSO iterations
2. Calculate the inverse solution of the particle by (45)
3. The objective function values of all particles and their reverse solutions were computed, and the optimal M particles were selected as their initial positions
4. Initialize $Z_i(t)$ and $Z_g(t)$, and then update Z_{mbst}^t and $z_i(t)$
5. Calculate the objective function values of the particles
6. Mutation operation is performed on particles by (41)
7. The fitness value of the current particle is calculated using (37) and compared with the individual optimal fitness value. The individual optimal position with a lower fitness is selected for updating the individual optimal value $Z_i(t)$

8. The current fitness value of the particle is compared with the swarm optimal fitness value, and the position with a smaller fitness value is selected as the new swarm optimal fitness value, and updated $Z_g(t)$
9. Let $t = t + 1$, the output condition being met, $Z_g(t)$ shall be outputted; otherwise, return to step 2
10. end

3.5 PFDL-IMFAC based on EQPSO parameter optimization

In the control scheme outlined in Fig. 2, the EQPSO algorithm is utilized to dynamically optimize the parameters of the PFDL-IMFAC controller. By considering the controller parameters as optimization variables within the EQPSO algorithm framework, appropriate values for these parameters are determined using a proposed fitness function.

Based on previous experimental verification, it has been determined that the parameters of $\lambda, \mu, \eta, \rho_i (i = 1, 2, 3), \Xi_{ii1}(0), \Xi_{ij1}(0)$ significantly affect the performance of the controller. Therefore, this study adopts these parameters as the optimization variables in the EQPSO algorithm to identify suitable controller parameters for the current system based on a proposed fitness function.

The main parameters of EQPSO are set as follows: the population size $M = 20$, the maximum number of iterations $I_{max} = 20$, and the maximum and minimum values of the particles are set as $x_{ij}^{low} = 0.1$ and $x_{ij}^{up} = 10$, respectively; the EQPSO error threshold is set as 10^{-3} .

The pseudo-code algorithm procedure of the PFDL-IMFAC is presented in Algorithm 2.

Algorithm 2 EQPSO-PFDL-IMFAC controller pseudo code

Input: The historical input and output data of the control system are denoted as $u(k), T(k)$, while the desired strip temperature is represented by $T_m(k)$. Additionally, the termination conditions and constraints are taken into consideration

Output: The actual strip temperature at the outlet of CAF is $T(k + 1)$;

1. Initialized the controller parameters $\lambda, \mu, \eta, \rho_i (i = 1, 2, 3), \Xi_{i1}(0), \Xi_{ij1}(0)$;
2. for $i = 1, 2, \dots, I_{max}$ do;
3. Using the EQPSO optimization algorithm, the current control step parameter values are $\lambda, \mu, \eta, \rho_i (i = 1, 2, 3), \Xi_{i1}(0), \Xi_{ij1}(0)$;
4. The value of $\hat{\Xi}_{pq}(k)$ can be determined by (12);
5. According to (17), the control variable $\Delta u(k)$ is obtained;
6. The current step control quantity $u(k)$ can be calculated using (10), and then substituted into (5) to obtain the actual output $T(k)$ of the system;
7. end

Figure 3 is the fitness curve graph, it can be seen from Fig. 3 that after 8 iterations, the adaptive degree function converges to a fixed value.

The PFDL-IMFAC improved by the EQPSO algorithm, along with the fixed parameter MFAC and the PID parameter values participating in the comparison, are presented in Table 1. Here, $K_p, K_I,$ and K_D denote the PID controller parameters; fuT and vsp represent the furnace temperature regulator and the strip speed regulator, respectively. The Nonlinear MPC (NMPC)

method is employed for comparative experiments, as outlined in reference [29], with parameter selection based on the recommendations from this document.

4 Analysis of simulation results

To evaluate the effectiveness of the PFDL-IMFAC scheme, this study conducted a series of MATLAB simulation experiments. In these experiments, four control methods—PID controller (as described in reference [28]), NMPC (in [29]), PFDL-MFAC, and the proposed PFDL-IMFAC—were assessed using the same model for output data generation. Additionally, the correlations between strip temperature, furnace temperature, strip speed, and fuel loss were analyzed. To accurately reflect on-site production phenomena, the reference input is given by

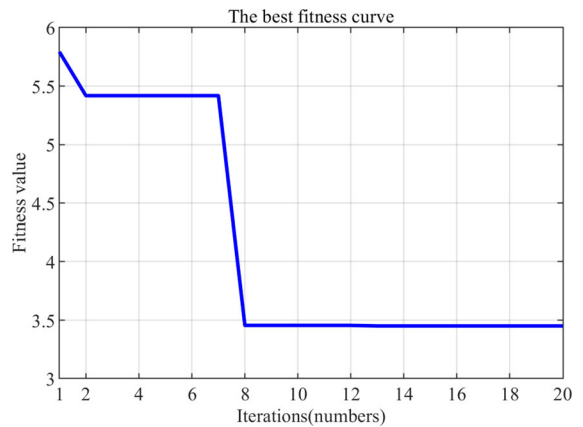


Fig. 3 The best fitness curve of EQPSO

Table 1 Controller parameters settings

Control algorithms	PFDL-MFAC	PFDL-IMFAC	PID
$\Xi_{11}(0), \Xi_{12}(0)$	1,2	0.5280,1.6643	$K_p^{fuT} = 1.7190$
$\Xi_{21}(0), \Xi_{22}(0)$	1,2	0.6795,0.7328	$K_I^{fuT} = 0.4819$
$\Xi_{31}(0), \Xi_{32}(0)$	1,2	1.4384,1.9809	$K_D^{fuT} = 3.2428$
η	1	2	$K_p^{vsp} = 9.4455$
μ	1	0.6472	$K_I^{vsp} = 3.1005$
ρ_i	0.8	0.4	$K_D^{vsp} = 0$
λ	1	2.8216	–
ζ	0	0.001	–

Table 2 Comparison of intelligent algorithms

Intelligent algorithms	RMSE	Energy loss	Savings rate
PID	28.069	2.9219e + 9	–
NMPC	16.152	2.9013e + 9	0.0071
PFDL-MFAC	10.082	2.8892e + 9	0.0112
PFDL-IMFAC	13.608	2.7962e + 9	0.0430

$$T_m(k) = \begin{cases} 682.0, & (0 < k \leq 240 \& 2640 < k \leq 2880) \\ 747.6, & (960 < k \leq 1200 \& 2400 < k \leq 2640) \\ 764.0, & (240 < k \leq 480 \& 1680 < k \leq 1920 \dots \\ \& 2160 < k \leq 2400, 2880 < k \leq 3120, 3840 < k \leq 4080) \\ 780.4, & (1200 < k \leq 1440 \& 3120 < k \leq 3360, 4080 < k \leq 4800) \\ 813.2, & (720 < k \leq 960 \& 1440 < k \leq 1680 \& 3360 < k \leq 3600) \\ 846.0, & (480 < k \leq 720 \& 1920 < k \leq 2160 \& 3600 < k \leq 3840). \end{cases} \tag{46}$$

The control performances of four different control methods are presented in Table 2. To visually evaluate the effectiveness of the controller, two performance indicators, namely root mean square error (RMSE) and energy loss W , are utilized for assessment. The calculation formulas for these indicators are presented in (47), where u_k is the control input. According to the process requirements, the strip speed and the CAF temperature are within the ranges of 0 ~ 550 m/min and 500 ~ 900°C, respectively. It is evident that both the PFDL-MFAC and PFDL-IMFAC schemes demonstrate similar control performances. However, the PFDL-IMFAC scheme is distinguished as the most energy-efficient, achieving a notable energy savings of 4.3% compared with PID controller.

$$\begin{cases} RMSE = \frac{1}{M} \sqrt{\sum_{k=1}^M |T_m(k) - T(k)|^2} \\ W = \sum_{k=1}^M u_k^2. \end{cases} \tag{47}$$

The comparison of the strip temperatures using PID, NMPC, PFDL-MFAC, and PFDL-IMFAC is illustrated in Fig. 4, while Fig. 5 presents the error comparison between actual and expected strip temperatures. According to Figs. 4 and 5, using the PID controller results in more significant fluctuations in the annealing temperature of the steel strip due to variations in its specifications, compared to the NMPC, PFDL-MFAC, and PFDL-IMFAC controllers. These fluctuations significantly impact the yield rate of steel strip products. For precise temperature control of the steel strip, the PFDL-MFAC and PFDL-IMFAC controllers outperform the PID and NMPC controllers.

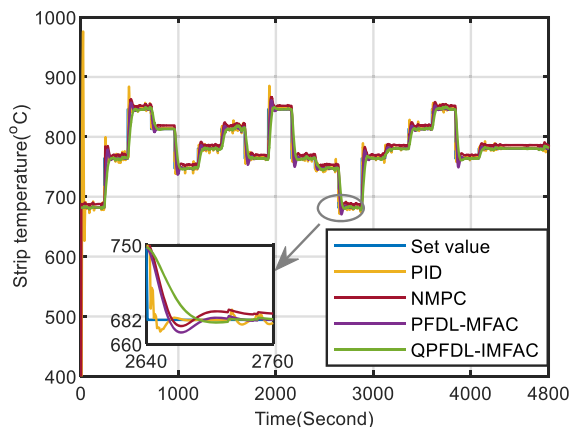


Fig. 4 Strip temperature curve at the outlet of CAF

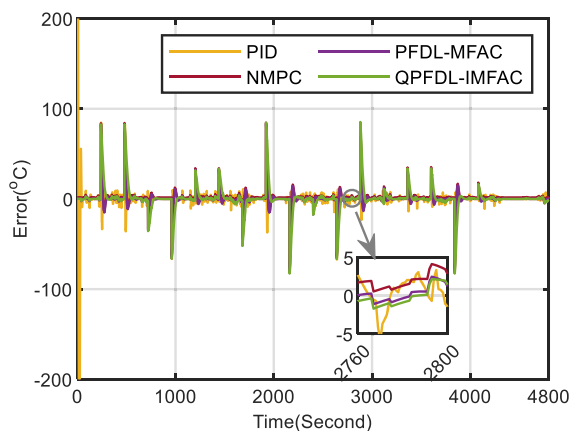


Fig. 5 Strip temperature error curve

Furthermore, the PFDL-IMFAC controller provides smoother transitions in control effects when switching between different steel strip specifications.

The curves depicted in Figs. 6 and 7 demonstrate the fluctuations in furnace temperature and strip speed for the CAF equipped with PID, NMPC, PFDL-MFAC, and PFDL-IMFAC controllers, respectively. The annealing temperature of the strip is controlled by adjusting the furnace temperature and the strip speed. Based on the findings presented in Fig. 6, it is evident that the furnace’s required temperature is higher when using PID, NMPC, and PFDL-MFAC controllers compared to PFDL-IMFAC, leading to increased fuel consumption for PID, NMPC, and PFDL-MFAC controllers. Notably, the PID controller results in more frequent temperature fluctuations in the furnace, suggesting instability and diminished robustness. Figure 7 shows the adjustment of strip speed,

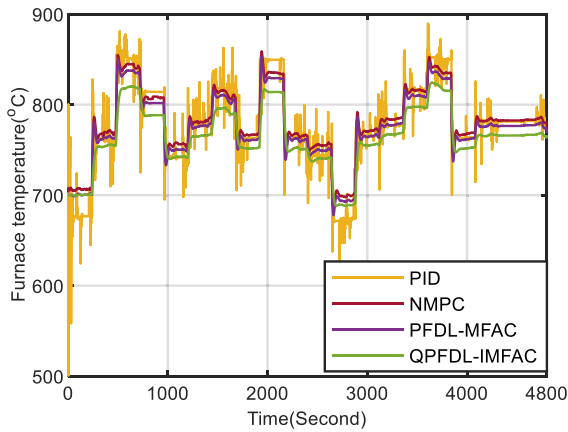


Fig. 6 CAF temperature change curve

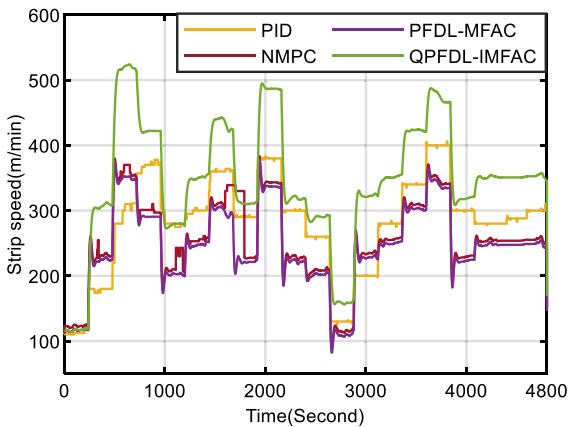


Fig. 7 Strip speed set value change curve in CAF

revealing that PFDL-IMFAC achieves significantly higher average strip speeds than other controllers while maintaining precise steel strip annealing temperatures. The findings indicate that the utilization of PFDL-IMFAC within the acceptable parameters of continuous annealing line speeds and furnace temperature has the potential to improve product output and fuel efficiency.

The plot illustrating the variation of PPD in PFDL-MFAC can be observed in Fig. 8. It can be inferred that the optimal initial value of PPD can be obtained by employing the EQPSO algorithm to achieve the most efficient control. The PPD consistently regulates the strip temperature in response to variations in its specifications.

From the above analysis, it can be concluded that the proposed PFDL-IMFAC control scheme can optimize the fuel utilization efficiency of CAF and

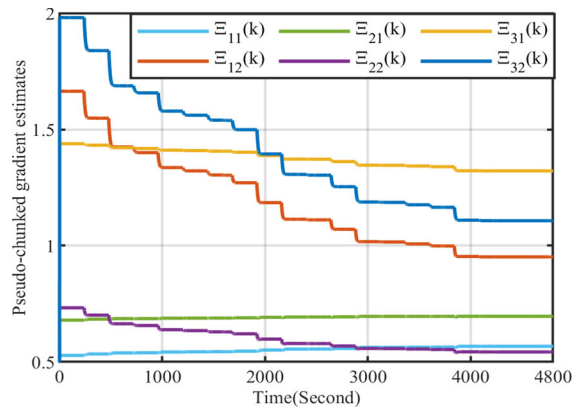


Fig. 8 PPD change graph

increase the unit capacity while ensuring the accurate annealing precision of the strip.

5 Conclusion

This study has proposed an improved model-free adaptive control method based on a partial form dynamic linearization and solved the temperature control problem of the steel strip with a continuous annealing furnace. By introducing the quantum-behaved particle swarm optimization algorithm for dynamic parameter adjustment, the system could be adapted to changes in external interferences effectively. To improve the energy efficiency of the continuous annealing furnace, an energy penalty function has been incorporated into the criterion function. The simulation results have shown that the PFDL-IMFAC control scheme has superior control performance compared to the PID and PFDL-MFAC control schemes. In conclusion, the proposed control scheme effectively meets the specific requirements of industrial processes, providing valuable insights for improving industrial production quality and increasing finished product output. Regrettably, the study failed to consider the interaction effects between the heating segment of the CAF and its adjacent processes. This oversight highlights a critical area for future research: the exploration of refined methods for integrated decision-making and control. Such methods should aim at achieving fully automated and intelligent production within the CAF system. By employing these advanced strategies, we can expect significant

improvements in efficiency and quality control throughout the manufacturing process [43, 44].

Author contributions H. Ding, Q. Xie, Ju H. Park, and H. Shen wrote the main manuscript text. All authors reviewed the manuscript.

Funding This work was supported by the National Natural Science Foundation of China under grant numbers 62273006, 62173001, 61873002, and 61703004, Distinguished Young Scholars of Higher Education Institutions of Anhui Province under grant 2022AH020034, the Natural Science Foundation for Excellent Young Scholars of Higher Education Institutions of Anhui Province under grant 2022AH030049, the research and development project of Engineering Research Center of Biofilm Water Purification and Utilization Technology of Ministry of Education under Grant BWPU2023ZY02, the University Synergy Innovation Program of Anhui Province under Grant GXXT-2023-020. And this work of J.H. Park was supported by the National Research Foundation of Korea (NRF) grant funded by the Korea government (Ministry of Science and ICT) (No. 2019R1A5A8080290).

Data availability No datasets were generated or analysed during the current study.

Declarations

Conflict of interest The authors declare no competing interests.

References

- Ji, C., Wang, L., Zhu, M.Y.: Effect of subcritical annealing temperature on microstructure and mechanical properties of SCM435 steel. *J. Iron. Steel Res. Int.* **22**, 1031–1036 (2015)
- Cui, H.R., Lai, J.P., Pan, Q.L., Wang, X.D.: Effect of N and Zr on as-cast microstructure and properties after annealing of a high-speed steel. *J. Iron. Steel Res. Int.* **25**, 460–468 (2018)
- Yi, Z., Su, Z.G., Li, G.J., Yang, Q.D.: Development of a double model slab tracking control system for the continuous reheating furnace. *Int. J. Heat Mass Transf.* **113**, 861–874 (2017)
- Huo, P.D., Li, F., Wang, Y., Wu, R.Z.: Annealing coordinates the deformation of shear band to improve the microstructure difference and simultaneously promote the strength-plasticity of composite plate. *Materials. Design.* **219**, 110696 (2022)
- Lin, K., Pourmajidian, M., Suleiman, F.K., McDermid, J.R.: Effect of annealing atmosphere and steel alloy composition on oxide formation and radiative properties of advanced high-strength steel strip. *Metall. Mater. Trans. B.* **53**, 380–393 (2022)
- Wang, X.P., Dong, Z.M., Tang, L.X., Zhang, Q.F.: Multi-objective multitask optimization-neighborhood as a bridge for knowledge transfer. *IEEE Trans. Evol. Comput.* **27**, 155–169 (2023)
- Zhao, Y.B., Song, Y., Li, F.F., Yan, X.L.: Prediction of mechanical properties of cold rolled strip based on improved extreme random tree. *J. Iron. Steel Res. Int.* **30**, 293–304 (2023)
- Zhang, Y.Y., Cao, W.H., Qu, Q.L.: Multi-objective optimization for gas distribution in continuous annealing process. *J. Adv. Comput. Intell.* **23**, 229–235 (2019)
- Yu, J.J., Sang, W.K.: An estimation of a billet temperature during reheating furnace operation. *Int. J. Control Auto. Syst.* **5**, 43–50 (2007)
- Li, G.J., Ji, W.C., Wei, L.Y., Yi, Z.: A novel fuel supplies scheme based on the retrieval solutions of the decoupled zone method for reheating furnace. *Int. Commun. Heat Mass Transf.* **141**, 106572 (2023)
- Wang, Y., Wang, X.P.: A dual-population multiobjective co-evolutionary matching ensemble learning for product multi-indicator prediction in continuous annealing. *Neurocomputing* **572**, 127226 (2024)
- Yu, H., Gong, J.N., Wang, G.Y., Chen, X.F.: A hybrid model for billet tapping temperature prediction and optimization in reheating furnace. *IEEE Trans. Ind. Inform.* **19**, 8703–8712 (2023)
- Bao, Q.F., Zhang, S., Guo, J., Li, Z.Q.: Multivariate linear-regression variable parameter spatio-temporal zoning model for temperature prediction in steel rolling reheating furnace. *J. Process Contr.* **123**, 108–122 (2023)
- Elsisi, M., Altius, M., Su, S.F., Su, C.L.: Robust Kalman filter for position estimation of automated guided vehicles under cyberattacks. *IEEE Trans. Instrum. Meas.* **72**, 1002612 (2023)
- Suid, M.H., Ahmad, M.A.: Optimal tuning of sigmoid PID controller using nonlinear sine cosine algorithm for the automatic voltage regulator system. *ISA Trans.* **128**, 265–286 (2022)
- Lui, D.G., Petrillo, A., Santini, S.: Leader tracking control for heterogeneous uncertain nonlinear multi-agent systems via a distributed robust adaptive PID strategy. *Nonlinear Dyn.* **108**(1), 363–378 (2022)
- Gupta, S.K., Wang, J., Barry, O.R.: Nonlinear vibration analysis in precision motion stage with PID and time-delayed feedback controls. *Nonlinear Dyn.* **101**, 439–464 (2020)
- Zhang, L., Jiang, Y., Chen, G., Tang, Y., Lu, S., Gao, X.: Heading control of variable configuration unmanned ground vehicle using PID-type sliding mode control and steering control based on particle swarm optimization. *Nonlinear Dyn.* **111**(4), 3361–3378 (2023)
- Taghieh, A., Mohammadzadeh, A., Zhang, C.W., Rathinasamy, S.: A novel adaptive interval type-3 neuro-fuzzy robust controller for nonlinear complex dynamical systems with inherent uncertainties. *Nonlinear Dyn.* **111**(1), 411–425 (2023)
- Ren, Y.Y., Ding, D.W., Li, Q., Xie, X.P.: Static output feedback control for T-S fuzzy systems via a successive convex optimization algorithm. *IEEE Trans. Fuzzy Syst.* **30**, 4298–4309 (2022)
- Zhai, J.C., Wang, H.Q., Tao, J.Q., He, Z.W.: Observer-based adaptive fuzzy finite time control for non-strict

- feedback nonlinear systems with unmodeled dynamics and input delay. *Nonlinear Dyn.* **111**(2), 1417–1440 (2023)
22. Wang, J., Krstic, M.: Event-triggered adaptive control of coupled hyperbolic PDEs with piecewise-constant inputs and identification. *IEEE Trans. Autom. Control* **68**, 1568–1583 (2023)
 23. Deng, C., Wen, C.Y., Wang, W., Li, X.Y.: Distributed adaptive tracking control for high-order nonlinear multi-agent systems over event-triggered communication. *IEEE Trans. Autom. Control* **68**, 1176–1183 (2023)
 24. Dai, C.B., Xue, Y.L., Wu, Z.L., Yan, G.Y.: Active disturbance rejection control for the reheated steam temperature of a double-reheat boiler. *J. Process Contr.* **130**, 103078 (2023)
 25. Xu, Y.L., Ding, C.Y., Su, X.Y., Li, Z.: Predictive-adaptive sliding mode control method for reluctance actuator maglev system. *Nonlinear Dyn.* **111**(5), 4343–4356 (2023)
 26. Agajie, T.F., Fopah-Lele, A., Ali, A., Amoussou, I.: Optimal sizing and power system control of hybrid solar PV-biogas generator with energy storage system power plant. *Sustainability.* **15**(7), 5739 (2023)
 27. Elsis, M.: Optimal design of adaptive model predictive control based on improved GWO for autonomous vehicle considering system vision uncertainty. *Appl. Soft Comput.* **158**, 111581 (2024)
 28. Rivera, D.E., Morari, M., Skogestad, S.: Internal model control: PID controller design. *Ind. Eng. Chem. Process Des. Develop.* **25**(1), 252–265 (1986)
 29. Wu, H., Speets, R., Ozcan, G., Ekhart, R.: Non-linear model predictive control to improve transient production of a hot dip galvanising line. *Ironmak. Steelmak.* **43**, 541–549 (2016)
 30. Niederer, M., Strommer, S., Steinboeck, A., Kugi, A.: Nonlinear model predictive control of the strip temperature in an annealing furnace. *J. Process Contr.* **48**, 1–13 (2016)
 31. Hou, Z.S., Jin, S.T.: A novel data-driven control approach for a class of discrete-time nonlinear systems. *IEEE Trans. Control Syst. Technol.* **19**, 1549–1558 (2011)
 32. Hou, Z.S., Xiong, S.S.: On model-free adaptive control and its stability analysis. *IEEE Trans. Autom. Control* **64**, 4555–4569 (2019)
 33. Elsis, M., Zaini, H.G., Mahmoud, K., Shima, B.: Improvement of trajectory tracking by robot manipulator based on a new co-operative optimization algorithm. *Mathematics.* **9**(24), 3231 (2021)
 34. Mohamed, M.A.E., Mohamed, S.M.R., Saied, E.M.M., Elsis, M.: Optimal energy management solutions using artificial intelligence techniques for photovoltaic empowered water desalination plants under cost function uncertainties. *IEEE Access.* **10**, 93646–93658 (2022)
 35. Essa, M.E.S.M., Elsis, M., Elsayed, M.S., Ahmed, M.F.: An improvement of model predictive for aircraft longitudinal flight control based on intelligent technique. *Mathematics* **10**(19), 3510 (2022)
 36. Bergies, S., Su, S.F., Elsis, M.: Model predictive paradigm with low computational burden based on dandelion optimizer for autonomous vehicle considering vision system uncertainty. *Mathematics.* **10**(23), 4539 (2022)
 37. Li, F.H., Hou, Z.S.: Distributed model-free adaptive control for MIMO nonlinear multiagent systems under deception attacks. *IEEE Trans. Syst. Man Cybern. -Syst.* **53**, 2281–2291 (2023)
 38. Kumar, N., Mahato, S.K., Bhunia, A.K.: A new QPSO based hybrid algorithm for constrained optimization problems via tournamenting process. *Soft. Comput.* **24**, 11365–11379 (2020)
 39. Xing, Z.Y., Zhu, J.L., Zhang, Z.Y., Qin, Y.: Energy consumption optimization of tramway operation based on improved PSO algorithm. *Energy* **258**, 124848 (2022)
 40. Deng, W., Ni, H.C., Liu, Y., Chen, H.L.: An adaptive differential evolution algorithm based on belief space and generalized opposition-based learning for resource allocation. *Appl. Soft Comput.* **127**, 109419 (2022)
 41. Li, J.Y., Du, K.J., Zhan, Z.H., Wang, H.: Distributed differential evolution with adaptive resource allocation. *IEEE Trans. Cybern.* **53**, 2791–2804 (2023)
 42. Li, Z.Q., Zhou, L., Yang, H.: Data-driven model-free adaptive control method for high-speed electric multiple unit. *Acta Auto. Sin.* **49**, 437–447 (2023)
 43. Liu, J., Gao, Y., Yin, Y., Wang, J., Sun, G.: *Sliding Mode Control Methodology in the Applications of Industrial Power Systems*, p. 205. Springer International Publishing, Switzerland (2020)
 44. Ma, L., Cheng, C., Guo, J., Shi, B., Ding, S., Mei, K.: Direct yaw-moment control of electric vehicles based on adaptive sliding mode. *Math. Biosci. Eng.* **20**(7), 13334–13355 (2023)

Publisher's Note Springer Nature remains neutral with regard to jurisdictional claims in published maps and institutional affiliations.

Springer Nature or its licensor (e.g. a society or other partner) holds exclusive rights to this article under a publishing agreement with the author(s) or other rightsholder(s); author self-archiving of the accepted manuscript version of this article is solely governed by the terms of such publishing agreement and applicable law.